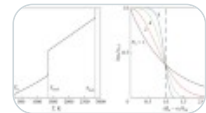


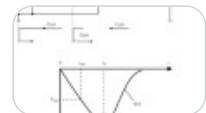
25 articles in this issue

Possibility of Changing the Plasma Formation Time during Conductor Electrical Explosion in the Skin Mode



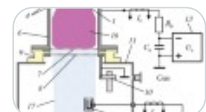
OriginalPaper | 13 January 2026 | Pages: S183 - S189

Contraction of Self-Sustained Subnanosecond Discharge



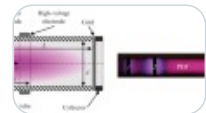
OriginalPaper | 13 January 2026 | Pages: S190 - S196

Operation Features of a Planar Magnetron Discharge Forming Emission Plasma in a Pulsed Forevacuum Plasma-Cathode Electron-Beam Source



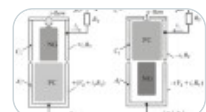
OriginalPaper | 13 January 2026 | Pages: S197 - S205

Plasma Diffuse Jet in Dielectric Tube as the Laboratory Analogue of Red Sprites



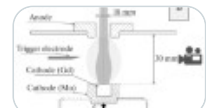
OriginalPaper | 13 January 2026 | Pages: S206 - S211

Parasitic Current in a Pseudospark Switch at Different Electric Circuits for Powering the Auxiliary Glow Discharge



OriginalPaper | 13 January 2026 | Pages: S212 - S217

Transient Processes during the Initiation and Stabilization of a Diffuse Vacuum Arc Discharge on a Gadolinium Cathode



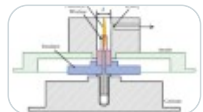
OriginalPaper | 13 January 2026 | Pages: S218 - S224

Spectral Energy Characteristics' Study of Coaxial Ablative Pulsed Plasma Accelerator



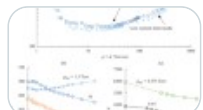
OriginalPaper | 13 January 2026 | Pages: S225 - S230

Structure of Plasma Jets Formed by a High-Current Vacuum Arc Discharge



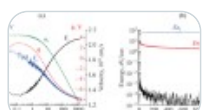
OriginalPaper | 13 January 2026 | Pages: S231 - S237

Breakdown Characteristics in Direct Current Discharge in Noble Gases



OriginalPaper | 13 January 2026 | Pages: S238 - S244

Suprathermal Electrons in Expanding Plasma of Vacuum Arc Jet



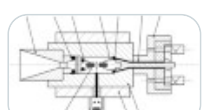
OriginalPaper | 13 January 2026 | Pages: S245 - S250

Double Pulse Effect in the Initiation of Runaway Electron Emission in an Air Gap



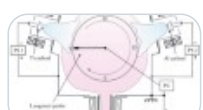
OriginalPaper | 13 January 2026 | Pages: S251 - S258

Numerical Simulation of the Shock Wave Propagation in the Discharge Chamber with Megaampere Discharge in High Density Gas



OriginalPaper | 13 January 2026 | Pages: S259 - S263

Numerical Simulation of Plasma Formation in a Hollow Anode with Metal Plasma Arc Evaporators



OriginalPaper | 13 January 2026 | Pages: S264 - S269

Influence of an Axial Magnetic Field on the Charged Particle Flow from a Conical Cathode in a Gas under Space-Charge-Limited Current Conditions



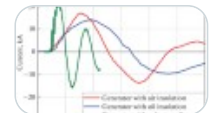
OriginalPaper | 13 January 2026 | Pages: S270 - S276

Discharge Plasma Parameters of Magnetron Sputtering System in Gas and Vacuum (Gasless) Operating Modes



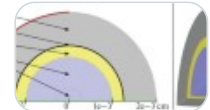
OriginalPaper | 13 January 2026 | Pages: S277 - S283

Using Generators with Operating Voltage of 50 kV for Electric Discharge Crushing of Quartz Raw



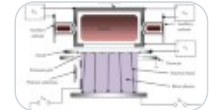
OriginalPaper | 13 January 2026 | Pages: S284 - S288

Dynamics of a Microsphere with a Double-Layer Shell in a Polymeric Matrix under the Impact of a Shock Wave



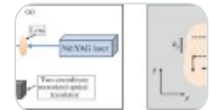
OriginalPaper | 13 January 2026 | Pages: S289 - S293

Ribbon Electron Beam for Generation of Beam Plasma and Beam-Plasma Treatment of Polymers in the Pressure Range of 0.1–10 Pa



OriginalPaper | 13 January 2026 | Pages: S294 - S301

The Influence of UV Laser Treatment on the Structure and Surface Properties of Ti–6Al–4V Titanium Alloy



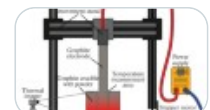
OriginalPaper | 13 January 2026 | Pages: S302 - S310

Plasma Chemical Reactor for the Synthesis of Lanthanum Hexaboride



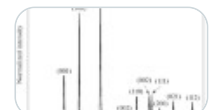
OriginalPaper | 13 January 2026 | Pages: S311 - S317

Characteristics of Temperature Field Distribution during Vacuum-Free Electric Arc Synthesis



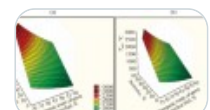
OriginalPaper | 13 January 2026 | Pages: S318 - S324

Oxidation Properties of High-Entropy Boride $(\text{Ti}_{0.2}\text{Zr}_{0.2}\text{Nb}_{0.2}\text{Hf}_{0.2}\text{Ta}_{0.2})\text{B}_2$ Synthesized by DC Arc Discharge Plasma



OriginalPaper | 13 January 2026 | Pages: S325 - S331

Plasma Utilization and Immobilization of Waste Reprocessing for Spent Nuclear Fuel



OriginalPaper | 13 January 2026 | Pages: S332 - S340

Raman Spectroscopy of the Petroleum Asphaltenes and Their Oxidation Products



Structure of Supramers Formed by Glycolipid Analogues: SAXS Study

